The infrared absorption spectrum of phenylacetylene and its deuterated isotopologue in the mid- to far-IR

Esposito, V.J.; Ferrari, P.; Buma, W.J.; Fortenberry, R.C.; Boersma, C.; Candian, A.; Tielens, A.G.G.M.

The Journal of Chemical Physics

RESEARCH ARTICLE | MARCH 19 2024

The infrared absorption spectrum of phenylacetylene and its deuterated isotopologue in the mid- to far-IR

Special Collection: 2024 JCP Emerging Investigators Special Collection

Vincent J. Esposito ; Piero Ferrari ; Wybren Jan Buma ; Ryan C. Fortenberry ; Christiaan Boersma ; Alessandra Candian ; Alexander G. G. M. Tielens

J. Chem. Phys. 160, 114312 (2024)
https://doi.org/10.1063/5.0191404

AIP Publishing

The Journal of Chemical Physics ARTICLE pubs.aip.org/aip/jcp

The infrared absorption spectrum of phenylacetylene and its deuterated isotopologue in the mid- to far-IR

Cite as: J. Chem. Phys. 160, 114312 (2024); doi: 10.1063/5.0191404
Submitted: 13 December 2023 • Accepted: 18 February 2024 •
Published Online: 19 March 2024

Vincent J. Esposito,[1,a] Piero Ferrari,[2] Wybren Jan Buma,[2,3] Ryan C. Fortenberry,[4] Christiaan Boersma,[1] Alessandra Candian,[5] and Alexander G. G. M. Tielens[6,7]

AFFILIATIONS

[1] NASA Ames Research Center, MS 245-6, Moffett Field, California 94035, USA
[2] Radboud University, Institute for Molecules and Materials, HFML-FELIX, 6525 ED Nijmegen, The Netherlands
[3] Van't Hoff Institute for Molecular Sciences, University of Amsterdam, 1098 XH Amsterdam, The Netherlands
[4] Department of Chemistry and Biochemistry, University of Mississippi, University, Mississippi 38677-1848, USA
[5] Anton Pannekoek Institute for Astronomy, University of Amsterdam, 1098 XH Amsterdam, The Netherlands
[6] Leiden Observatory, Leiden University, 2333 CA Leiden, The Netherlands
[7] Astronomy Department, University of Maryland, College Park, Maryland 20742-2421, USA

Note: This paper is part of the 2024 JCP Emerging Investigators Special Collection.
[a] **Author to whom correspondence should be addressed:** Vincent.J.Esposito@nasa.gov

ABSTRACT

Anharmonicity strongly influences the absorption and emission spectra of polycyclic aromatic hydrocarbon (PAH) molecules. Here, IR–UV ion-dip spectroscopy experiments together with detailed anharmonic computations reveal the presence of fundamental, overtone, as well as 2- and 3-quanta combination band transitions in the far- and mid-infrared absorption spectra of phenylacetylene and its singly deuterated isotopologue. Strong absorption features in the 400–900 cm^{-1} range originate from CH(D) in-plane and out-of-plane wags and bends, as well as bending motions including the C≡C and CH bonds of the acetylene substituent and the aromatic ring. For phenylacetylene, every absorption feature is assigned either directly or indirectly to a single or multiple vibrational mode(s). The measured spectrum is dense, broad, and structureless in many regions but well characterized by computations. Upon deuteration, large isotopic shifts are observed. At frequencies above 1500 cm^{-1} for d_1-phenylacetylene, a one-to-one match is seen when comparing computations and experiments with all features assigned to combination bands and overtones. The C≡C stretch observed in phenylacetylene is not observed in d_1-phenylacetylene due to a computed 40-fold drop in intensity. Overall, a careful treatment of anharmonicity that includes 2- and 3-quanta modes is found to be crucial to understand the rich details of the infrared spectrum of phenylacetylene. Based on these results, it can be expected that such an all-inclusive anharmonic treatment will also be key for unraveling the infrared spectra of PAHs in general.

Published by AIP Publishing. https://doi.org/10.1063/5.0191404

I. INTRODUCTION

Polycyclic aromatic hydrocarbons (PAHs) are a class of molecules composed of fused hexagonal rings of sp^2-hybridized carbon atoms with hydrogens decorating the periphery, which are known to be ubiquitous in space based on their infrared emission features detected throughout many interstellar regions, i.e., the aromatic infrared bands (AIBs).[1,2] Recently, experimental and computational studies of the infrared absorption spectra of various PAHs have revealed large anharmonic effects. Previous attempts to account for anharmonicity included the use of harmonic scaling factors.[3–13] However, scaling factors do not account for important higher-order transitions such as combination bands and overtones, nor do they provide a good treatment of systems with a shallow minimum in their PESs.[14]

In cases where anharmonicity is strong, scaling factors are therefore not able to account for and accurately predict-infrared absorption spectra, in particular for regions that can only be

explained when anharmonic transitions such as combination bands are correctly taken into account.[8,15–23] At present, with the launch of the James Webb Space Telescope (JWST), very sensitive and high-resolution infrared spectral data of the PAH bands have and will continue to be delivered,[24] calling for a deeper understanding of anharmonic effects on the vibrational spectra of PAHs and how to take them into account in astronomical models. To do so, it requires a synergy between accurate computational modeling and sensitive laboratory spectroscopy experiments.

In the recent past, dedicated gas-phase experiments have been performed for a number of PAHs, and these indeed reveal that for these compounds, anharmonicity is essential to come to a proper interpretation of their infrared absorption spectra. For example, IR–UV ion-dip molecular beam experiments have been used to record infrared absorption spectra of neutral naphthalene, anthracene, tetracene, and pentacene, showing the appearance of many combination bands in the 1600–2000 cm^{-1} region.[17,18,25–28] Similarly, molecular beam experiments on the larger PAHs coronene, peropyrene, ovalene, and hexa(peri)benzocoronene have shown the presence of many combination bands and overtones in both the 1600–2000 and 2950–3150 cm^{-1} regions, whereas at lower frequencies (100 and 1000 cm^{-1}) fundamental transitions dominate.[29] Recently, using an infrared table-top laser system to cover the 3 μm spectral region, our research group performed ion-dip experiments on phenylacetylene and d_1-phenylacetylene (the singly deuterated isotopologue of phenylacetylene with deuteration taking place at the acetylene hydrogen),[16] representing an ideal model system to assess the impact of anharmonic effects on PAHs, in particular focusing on the possibility that higher-order quanta modes are a significant contributor to their infrared spectra. Remarkably, a major influence of 2- and 3-quanta modes arising from aromatic and acetylenic C–H and C–D stretching bands is observed.[16] Notably, phenylacetylene was recently detected in the dark molecular cloud TMC-1 via its pure rotational transitions,[30] making a detailed understanding of its infrared spectrum a pressing need.

In this work, the previous study is extended to the much larger 100–2300 cm^{-1} spectral range using an infrared free electron laser, thereby covering the far- and mid-infrared regions. Detailed anharmonic quantum chemical calculations are utilized to reveal the key role played by higher-order modes in shaping the infrared spectra.

II. METHODS

A. Experimental

Molecular beams of phenylacetylene and d_1-phenylacetylene are formed by placing the liquid compounds in a reservoir kept at room temperature that is seeded with a stream of Ar gas injected at a backing pressure of 4 bar. Using a Series 9 pulsed valve from General Valve, the Ar-phenylacetylene mixtures are expanded into vacuum, forming a cold and directional molecular beam that is collimated by a 2 mm skimmer. The pulsed valve is operated at 10 Hz. After collimation, the molecular beam enters the ionization region of a reflectron time-of-flight mass spectrometer (R. M. Jordan D-850) equipped with a 40 mm dual microchannel plate (MCP) detector (Jordan Co. C-726) that has a mass resolution of $m/\Delta m$ = 2200 at 100 amu. In previous studies on the same apparatus with similarly sized molecular systems, molecular dynamic simulations were used to compute infrared spectra at different temperatures, finding good agreement with a vibrational temperature of 50 K.[14] Similarly, previous estimations of the molecular beam temperature place its value in the range of 10 to 50 K.[31,32] Values much higher than this range would lead to visible hot bands in REMPI scans, which is not the case in the spectra in this study.

To measure mass spectra, phenylacetylene is ionized using a (1 + 1) Resonance Enhanced Two-Photon Ionization (R2PI) scheme. UV excitation is performed by the second harmonic light of a dye laser (Radiant Dye) pumped by the third harmonic of a Nd:YAG laser (InnoLas SpitLight1200) and operating on Coumarin 153 in ethanol. The laser system is tuned to the vibrationless origin of the $S_1 \leftarrow S_0$ electronic transition of each species occurring at 35 875.7 and 35 888.6 cm^{-1} for phenylacetylene and d_1-phenylacetylene, respectively.[16]

Infrared spectra are measured by ion-dip spectroscopy. For this, the laser light of the free electron laser FELIX is aligned counter-propagating with the molecular beam, as described in Ref. 33. Upon resonant vibrational excitation, depopulation of the vibrational ground-state leads to a reduction of the ion signal. Running the molecular beam instrument at 10 Hz and operating FELIX at 5 Hz then allows the consecutive measurement of mass spectra with and without FELIX excitation and, thereby, the recording of IR absorption spectra. Importantly, FELIX is timed 300 μs prior to the R2PI ionization, ensuring that vibrational excitation occurs when the molecules are in their neutral state. FELIX is tuned from 100 to 2300 cm^{-1} in steps of 1 cm^{-1}.

B. Computational

The computation of the optimized geometry, harmonic normal modes, and quadratic, cubic, and quartic normal coordinate force constants (quartic force field; QFF) is performed at the B3LYP[34]/N07D[35] level of theory utilizing the Gaussian 16 software package.[36] The computations were performed using very tight optimization criteria and a custom integration grid consisting of 200 radial shells and 974 angular points per shell (compared to 99 radial shells and 590 angular points per shell in the default ultrafine grid). The N07D basis set is based on the 6-31G(d) basis set and contains additional diffuse and polarization functions that have been shown to increase accuracy in the anharmonic computations of large aromatic systems such as PAHs.[37] A QFF is a truncated Taylor series expansion of the potential surface surrounding the equilibrium geometry, following the formula:

$$V = \frac{1}{2}\sum_{i,j}^{3N}\left(\frac{\partial^2 V}{\partial X_i \partial X_j}\right)X_i X_j + \frac{1}{6}\sum_{i,j,k}^{3N}\left(\frac{\partial^3 V}{\partial X_i \partial X_j \partial X_k}\right)X_i X_j X_k + \frac{1}{24}\sum_{i,j,k,l}^{3N}\left(\frac{\partial^4 V}{\partial X_i \partial X_j \partial X_k \partial X_l}\right)X_i X_j X_k X_l. \quad (1)$$

The QFF is computed in normal mode coordinates via a linear relationship to produce a Cartesian coordinate QFF. Additionally, semi-diagonal quartic terms are employed, as is the default in Gaussian 16.[38]

From here, two different methodologies are implemented via second order vibrational perturbation theory (VPT2).[39–42] Using the built-in anharmonic frequency code within Gaussian 16, VPT2 is used to compute the anharmonic frequencies, including up to three-quanta transitions. This allows for the inclusion of multi-mode combination bands that are imperative for an accurate analysis of the recorded experimental absorption data.

Alternatively, to properly treat the redistribution of intensity as a result of accidental resonances between vibrational states, a locally modified version of SPECTRO[43] is utilized to compute the anharmonic vibrational frequencies of transitions involving changes up to two vibrational quanta. SPECTRO has the advantage of using resonance polyads in the anharmonic computations.[44,45] When two vibrational states are close in frequency and produce a near-singularity in the VPT2 treatment, they are removed from the standard perturbation treatment and included in a resonance polyad matrix. The matrix allows for the treatment of resonance effects as well as normal modes that simultaneously participate in multiple resonances. Additionally, the polyad matrix allows for the distribution of intensities between coupled vibrational states. Vibrational modes with frequencies below 300 cm^{-1} are excluded from the SPECTRO VPT2 calculation. This method has been described previously in greater detail.[15–19,21,25]

The resultant vibrational absorption stick spectrum is convoluted with a Gaussian line shape having a full-width at half-maximum (FWHM) of 0.5% of the computational frequency, which matches the bandwidth of FELIX.

III. RESULTS AND DISCUSSION

A. Phenylacetylene absorption spectrum

Figure 1 presents the experimental infrared absorption spectrum (black) of phenylacetylene in the 100–2300 cm^{-1} frequency range, the harmonic stick spectrum (green), the 3-quanta anharmonic stick spectrum (purple), and the artificially broadened anharmonic spectrum (blue) based on this stick spectrum. The experimental band center, FWHM, and relative intensity, along with the pertinent associated computational anharmonic mode labeling, frequency, and intensity of the pertinent bands, are presented in Table I. The full list of computational frequencies and experimental transition assignments is provided in Table S1 of the supplementary material. The experimental transitions are determined via a least-squares fit using a Gaussian line shape. Overall, ~40 features can be identified from the experimental data above a signal-to-noise ratio of 2. Because of the resolution of the experiment, the many overlapping bands lead to unstructured, broad shapes and shoulders. Studying the computational spectrum leads to a deeper understanding as to why many of the features appear so broad and structureless. For example, in the experimental spectrum, the fit detected two

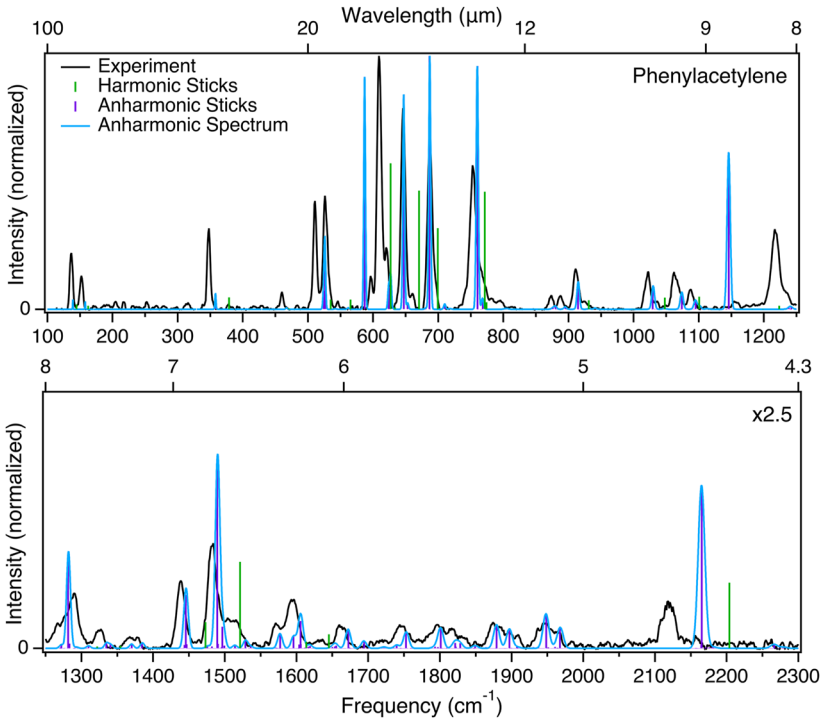

FIG. 1. Experimental (black), harmonic stick, and broadened anharmonic (blue; stick spectrum in purple) absorption spectra of phenylacetylene. The computed anharmonic spectrum in purple represents the stick spectrum convoluted with a Gaussian function with a FWHM of 0.5% of the computational frequency to reproduce the experimental linewidth of FELIX. The intensity in the lower panel has been multiplied by a factor of 2.5 to show details of the weaker features in this region.

TABLE I. Phenylacetylene mode number, anharmonic computational frequency (cm^{-1}), intrinsic intensity (km mol^{-1}), and relative intensity; and the experimental band centers (cm^{-1}), FWHM (cm^{-1}), and relative intensities.

Mode	Frequency (cm^{-1})	Intrinsic intensity (km mol^{-1})	Comp. rel. intensity[a]	Expt. band centers (cm^{-1})	FWHM Gaussian (cm^{-1})	Expt. rel. int.
ν_{21}	586.8	38.910	0.917	609.4	5.9	1.000
$\nu_{13} + \nu_{36}$	626.7	5.733	0.135	620.6	6.1	0.267
$\nu_{23} + \nu_{24} + \nu_{36}$	653.0	1.078	0.025	659.2	6.8	0.049
ν_{19}	760.3	40.727	0.960	753.1	8.4	0.588
ν_{12}	768.3	1.856	0.044	764.8	13.1	0.155
$\nu_{21} + \nu_{24} + \nu_{36}$	876.2	0.277	0.007	873.3	5.8	0.056
ν_{10}	1029.5	3.902	0.092	1021.8	7.8	0.138
ν_{32}	1073.9	2.855	0.067	1064.0	10.7	0.155
$\nu_{13} + \nu_{34}$	1095.3	1.536	0.036	1087.6	7.1	0.073
$2\nu_{21}$	1146.0	26.230	0.618	1217.6	11.6	0.267
ν_{7}	1489.6	12.538	0.296	1481.9	10.2	0.162
$2\nu_{21} + \nu_{33}$	1793.3	0.109	0.003	1795.9	18.6	0.037
$\nu_{14} + \nu_{15}$	1801.4	1.375	0.032			
$\nu_{14} + \nu_{18}$	1879.0	1.579	0.037	1875.4	15.5	0.037
$\nu_{17} + \nu_{18}$	1897.2	1.291	0.030			
$3\nu_{33}$	1907.5	0.092	0.002	1896.3	21.5	0.022
ν_{5}	2165.3	10.637	0.251	2119.0	18.0	0.078

[a]The computational relative intensities are in reference to the transition at 686.5 cm^{-1}, which is not listed here but can be found in Table S1 of the supplementary material.

neighboring features at 753.1 and 764.8 cm^{-1} within the broad feature centered at 753.1 cm^{-1}, which exhibits a shoulder on the high-frequency side. Using the anharmonic computations, these two features can be reliably assigned to ν_{19} [out-of-plane (OOP) aromatic CH wag] and ν_{12} (in-plane aromatic ring breathing mode), respectively, clearly explaining the finer details of the 753.1 cm^{-1} feature.

Across the entirety of the spectrum (Fig. 1), every experimental feature is assigned to either a single or multiple vibrational modes. Interestingly, the two features at 609.4 and 1217.6 cm^{-1} stand out as having poor agreement with the computations. The data in Table I show that the feature centered at 609.4 cm^{-1} is assigned to ν_{21}, which is the OOP acetylene CH wag that causes a large change in the dipole moment and leads to high intensity. The difference between the experiment and computed position for this mode is 22.6 cm^{-1}, larger than expected for a fundamental mode at this level of theory, especially considering that the surrounding features are well-described by the computations (e.g., the feature at 620.6 cm^{-1} is assigned to the $\nu_{13} + \nu_{36}$ combination band computed to be at 626.7 cm^{-1}). Anharmonic computations of OOP bending motions of aromatic systems consisting of sp^2 hybridized carbons have been previously reported to exhibit unexpected behavior when using density functional theory (DFT) methods in combination with some basis sets.[46] In this study, different DFT and correlated methods with varied basis sets were tested and all suffered the same issues with the OOP bending mode, and in fact, the B3LYP/N07D method performed the best against the experiment. Therefore, we believe that this is indeed the cause of the issue seen here. To confirm that there are no issues with basis set size, the harmonic vibrational spectrum of phenylacetylene calculated with B3LYP/N07D compares well to those calculated with B3LYP/6-311++G(d,p), agreeing to 16 cm^{-1} in the CH stretch region and ~4 cm^{-1} for lower frequency modes. The in-plane acetylene CH wag is slightly more sensitive to basis set size; however, a difference of ~3% will not impact the results in this study. Additionally, phenylacetylene has been reported to exhibit large couplings between various vibrational states of the acetylene substituent.[16] The initial error in the potential energy surface computation for ν_{21} is compounded when moving to higher-order transitions, along with the general decrease in accuracy when computing the frequency of overtone transitions (see Ref. 47 for more details). This leads to a larger error in the frequency for the feature centered at 1217.6 cm^{-1}, which arises from the first overtone of ν_{21} ($2\nu_{21}$). The other feature that has poor agreement between experiment and computation is the feature at 2119.0 cm^{-1}, assigned to ν_5 (2165.3 cm^{-1}), the acetylene C≡C stretch. It is unclear at the moment why there is such a large difference between experiment and theory for this feature.

Moving to higher frequencies, each feature from 1250 to 2000 cm^{-1} is assigned to one or more underlying modes. Due to the congested nature of this region, some features are assigned to multiple nearby modes that cannot be separated effectively. The harmonic stick spectrum (green) in Fig. 1 illustrates how important it is to include anharmonicity in the computations of the vibrational spectrum of PAHs. In the 1250–2000 cm^{-1} frequency range, only seven fundamental frequencies (green) exist, making it impossible to completely assign the complicated spectrum of phenylacetylene. However, when anharmonicity is included, hundreds of relatively intense overtone and combination bands

present themselves that agree quite nicely with the experimental features. Furthermore, the anharmonic intensities show better agreement with the experimental intensities than the double harmonic intensities do.

Figure 2 illustrates the 2-quanta (red) and 3-quanta (blue) vibrational modes computed for phenylacetylene. The importance of including the 3-quanta modes cannot be overstated, as can be seen from the figure and is highlighted by Table I. At least four 3-quanta modes (combination bands involving three fundamental vibrations or one fundamental mode and one overtone, as well as a second overtone mode) are assigned to features in the spectrum that would have been missed if the higher-order modes had not been included in the computations. For example, around 1800 cm^{-1}, the experiment reveals a double feature that can only be explained by including 3-quanta modes. Of note is that the 3-quanta computations are not performed with polyad matrices and, therefore, do not benefit from the proper treatment of intensity sharing. The less accurate intensities can be seen in the systematically larger intensity for almost all modes in the 3-quanta computations vs those of the 2-quanta in Fig. 2. A glaring example of this is the disappearance of the $2\nu_{21}$ feature in the 2-quanta computation. As the result of many strong resonance coupling interactions, the intrinsic intensity of this mode is redistributed over various nearby features. Not utilizing a polyad matrix will also affect the frequencies of the bands in the 3-quanta computations, although to a lesser degree. These issues will be addressed in subsequent studies when the capability to compute 3-quanta modes is further developed.

B. d_1-phenylacetylene absorption spectrum

Figure 3 presents the absorption spectrum of d_1-phenylacetylene in the range of 100–2300 cm^{-1} with the experiment shown in black, the harmonic stick spectrum in green, the anharmonic 3-quanta stick spectrum in purple, and the anharmonic stick spectrum broadened with a Gaussian lineshape (FWHM of 0.5% of the computational frequency) in blue. Table II lists the computational and experimental frequencies of prominent bands. The full list of experimental and computational frequencies is provided in Table S2 of the supplementary material. In the experimental spectrum, bands are observed throughout the spectral range, with mostly sharp, well-defined peaks below 800 cm^{-1} and broad, structure-less features above. The sole physical difference between phenylacetylene and d_1-phenylacetylene is a single deuteration, but this leads to major spectroscopic changes. Many spectral shifts originate from modes that involve the motion of the deuterium atom, and adjacent modes (such as the acetylene C≡C stretch) are also impacted. Here, theory provides insights into what drives these spectral changes.

There is generally good agreement between experiment and computation across the entire spectral range, with a few notable outliers. In the range from 450 to 560 cm^{-1}, there are four features present in the experimental spectrum, while theory predicts six bands. The three largest peaks in the experimental spectrum occur at 475.7, 480.6, and 527.2 cm^{-1}, with the peaks at 475.7 and 480.6 cm^{-1} overlapping (Fig. S1 shows an expanded view of this feature). An unambiguous assignment is difficult to make here, but the

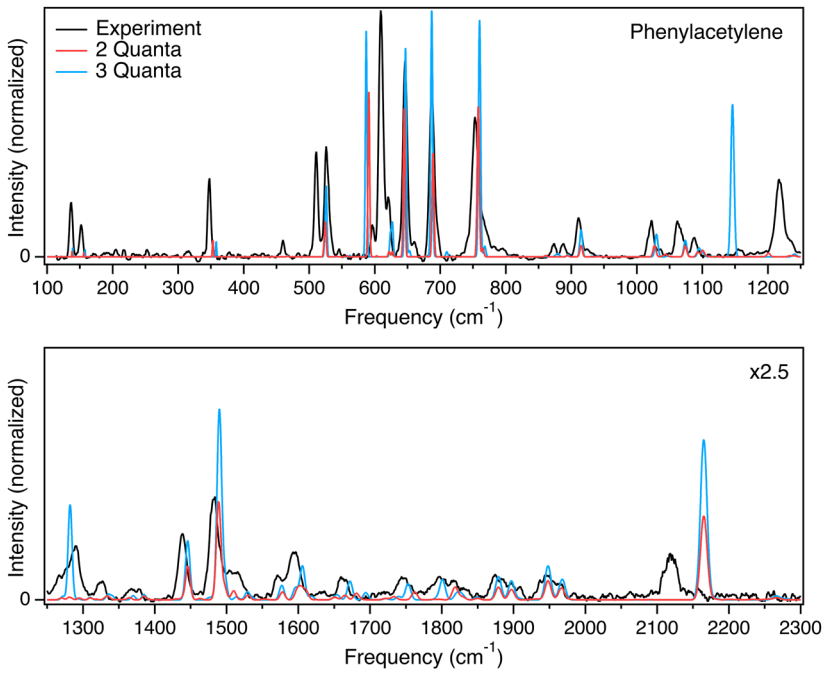

FIG. 2. Experimental (black), 3-quanta anharmonic (blue), and 2-quanta anharmonic (red) absorption spectra of phenylacetylene. The computed 3-quanta anharmonic spectrum shown in blue is convoluted with a Gaussian line shape with a linewidth equal to 0.5% of the computational frequency, reproducing the experimental linewidth of FELIX, while the 2-quanta anharmonic spectrum shown in red has a constant 1.0 cm^{-1} FWHM (for visualization purposes). The intensity in the lower panel has been multiplied by a factor of 2.5 to show details of the weaker features in this region.

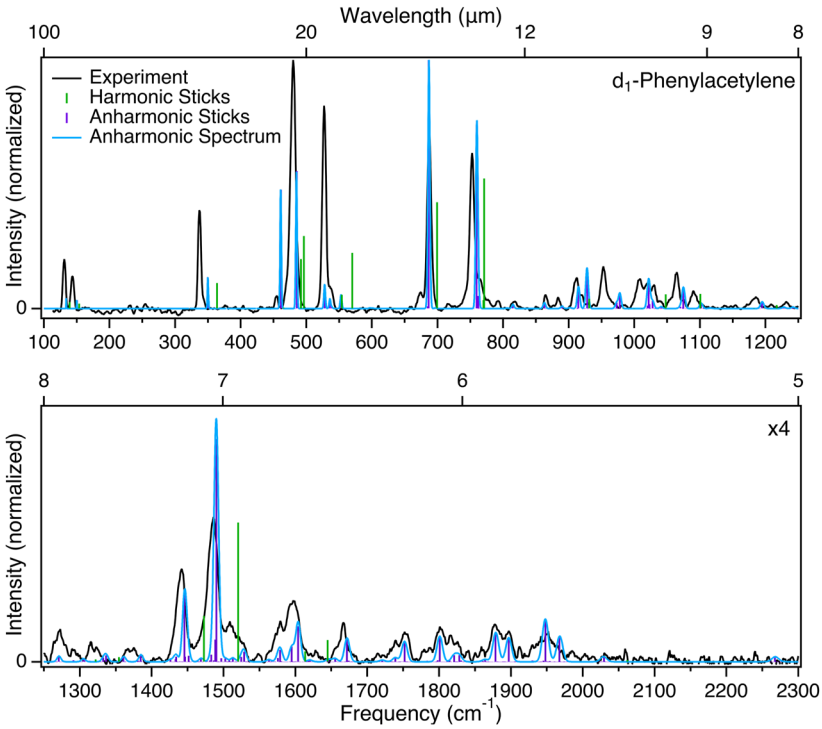

FIG. 3. Experimental (black), harmonic stick, and anharmonic (blue; stick spectrum in purple) absorption spectra of d_1-phenylacetylene. The computed anharmonic spectrum in blue represents the stick spectrum convolved with a Gaussian linewidth equal to 0.5% of the computational frequency to reproduce the experimental linewidth of FELIX. The intensity in the lower panel has been multiplied by a factor of 4 to show details of the weaker features in this region.

strongest peak at 480.6 cm^{-1} most likely originates from ν_{35}, which is the in-plane acetylene CD wag. ν_{22}, the OOP acetylene CD wag computed at 461.5 cm^{-1}, is tentatively assigned to the experimental feature at 475.7 cm^{-1}. This mode is analogous to ν_{21} in the standard isotopologue. Deuteration of the acetylene hydrogen leads to an experimental isotopic shift of 128.8 cm^{-1} for the OOP acetylene CH wag mode. Assigning the feature at 527.2 cm^{-1} is more difficult due to the three modes computed near the central peak position and the intensity mismatch. The carrier of this peak is probably ν_{21}, the OOP acetylene C≡C bend predicted at 528.1 cm^{-1}. After the VPT2 treatment, the computed intensity of ν_{21} drops from 18.229 km mol^{-1} (0.524 relative to ν_{20}) to 4.408 km mol^{-1} (0.097 relative to ν_{20}). As mentioned previously, OOP bending modes are sometimes not well described by DFT/VPT2, and intensities in general are difficult to calculate. Therefore, better agreement is found when considering the double harmonic intensities. Additionally, the lack of intensity sharing in these calculations contributes to the intensity mismatch for all of the features mentioned here. The other two small peaks predicted at 535.9 ($\nu_{16} + \nu_{24}$) and 539.1 (ν_{34}) cm^{-1} add to the intensity of the central peak and lead to the appearance of the shoulder on the high frequency side.

Moving to higher frequencies, there is somewhat less agreement between experiment and computation in the 900–1100 cm^{-1} range. However, ten prominent peaks are seen in both spectra, providing the ability to understand which modes are involved without directly assigning individual peaks. There is a mixture of transitions in this region characterized by fundamental, overtone, and 2- and 3-quanta combination bands contributing to features observed here; $2\nu_{22}$ reports the largest predicted intensity (see supplementary material Table S2). Only three fundamental transitions have appreciable intensity in this region (harmonic sticks in Fig. 3), indicating and reinforcing the strong impact of anharmonicity on phenylacetylene[16] and the need for anharmonic computations to properly analyze and understand its spectrum.

The broad feature centered at 1440.8 cm^{-1} with an FWHM of 11.9 cm^{-1} mainly originates from the ν_{28} aromatic CH in-plane bend fundamental transition. Underlying 2- and 3-quanta combination bands account for the remaining intensity that leads to the broadness of the feature. At higher frequencies, the experimental fit identifies three overlapping peaks at 1485.1, 1508.8, and 1521.9 cm^{-1} that make up the double peak feature around 1500 cm^{-1}. The two main modes here are the ν_7 aromatic CH in-plane bend fundamental as well as the $\nu_{10} + \nu_{13}$ combination band transition. Other higher-order overtone and combination band transitions contribute to the broad intensity and double peak structure.

From 1550 cm^{-1} upwards, there is an almost one-to-one match of experimental and computational features, all of which are higher-order modes (see also supplementary material Fig. S2). For example, $\nu_{18} + \nu_{19}$ is the combination band responsible for the experimental peak observed at 1666.4 cm^{-1}, while $\nu_{14} + \nu_{18}$ (1878.6 cm^{-1}) and $\nu_{17} + \nu_{18}$ (1897.2 cm^{-1}) are responsible for the bands observed experimentally at 1879.3 and 1896.8 cm^{-1}, respectively. The

TABLE II. d_1-Phenylacetylene mode number, anharmonic computational frequency (cm^{-1}), intrinsic intensity (km mol^{-1}), and relative intensity; and experimental band centers (cm^{-1}), FWHM (cm^{-1}), and relative intensities.[a]

Mode	Frequency (cm^{-1})	Intrinsic intensity (km mol^{-1})	Comp. rel. intensity[a]	Expt. band centers (cm^{-1})	FWHM Gaussian (cm^{-1})	Expt. rel. int.
ν_{22}	461.5	21.666	0.478	475.7	3.8	0.731
ν_{13}	461.7	0.245	0.005	454.3	2.0	0.079
ν_{35}	485.4	25.055	0.553	480.6	5.3	1.000
ν_{21}	528.1	4.407	0.097	527.2	4.8	0.828
$\nu_{16} + \nu_{24}$	535.9	1.785	0.039	537.2	5.8	0.082
ν_{34}	539.1	0.325	0.007			
$\nu_{21} + 2\nu_{22}$	1426.2	0.119	0.003	1440.8	11.9	0.104
$\nu_{14} + \nu_{22}$	1433.3	0.132	0.003			
$\nu_{18} + \nu_{21}$	1434.2	0.272	0.006			
ν_{28}	1445.5	3.588	0.079			
$\nu_{19} + \nu_{20}$	1446.6	0.270	0.006			
$\nu_{17} + \nu_{22}$	1451.4	0.321	0.007			
$2\nu_{21} + \nu_{22}$	1468.6	0.190	0.004			
$\nu_{13} + \nu_{34} + \nu_{35}$	1483.1	0.380	0.008			
$\nu_{10} + \nu_{13}$	1488.7	1.185	0.026	1485.1	14.7	0.160
ν_7	1490.2	11.941	0.264			
$\nu_8 + 2\nu_{36}$	1496.8	0.190	0.004	1508.8	9.5	0.043
$\nu_{13} + \nu_{20} + \nu_{23}$	1502.5	0.169	0.004			
$2\nu_{19}$	1512.9	0.209	0.005	1521.9	10.8	0.036
$2\nu_{12}$	1524.6	0.257	0.006			
$\nu_{15} + \nu_{20}$	1528.8	0.538	0.012			
$\nu_{10} + \nu_{34}$	1563.2	0.116	0.003	1576.6	12.0	0.029
$\nu_{20} + \nu_{23} + \nu_{34}$	1575.8	0.194	0.004			
ν_{27}	1578.8	0.642	0.014			
$\nu_{15} + \nu_{19}$	1594.9	0.812	0.018	1596.8	15.9	0.060
$\nu_{18} + \nu_{20}$	1603.9	0.240	0.005			
ν_6	1604.0	1.902	0.042			
$\nu_{14} + \nu_{18}$	1878.6	1.578	0.035	1879.3	13.0	0.031
$\nu_{17} + \nu_{18}$	1897.2	1.297	0.029	1896.8	8.5	0.025
ν_5	2029.5	0.277	0.006			

[a]The computational relative intensities are in reference to the transition at 686.6 cm^{-1}, which is not listed here but can be found in Table S2 of the supplementary material.

acetylene C≡C stretch (ν_5, 2029.5 cm^{-1}) is not observed in the spectrum of d_1-phenylacetylene due to a drop in intensity upon deuteration, contrasting with the fairly strong feature observed in the standard isotopologue.

IV. CONCLUSIONS

Anharmonicity is intrinsically required for the accurate characterization of the vibrational spectrum of polycyclic aromatic hydrocarbons,[16] a principle that is further supported by the results presented in the present study that cover frequencies from the mid- to far-infrared. For both phenylacetylene and d_1-phenylacetylene, direct and indirect assignments are only possible by including anharmonic terms in the vibrational potential energy surface calculation. The mid- to far-IR spectra of these molecules are full of higher-order transitions such as overtones and combination bands, including both 2- and 3-quanta combination bands. So far, 3-quanta bands have not received much attention. The present study demonstrates, however, that the inclusion of such transitions is necessary to come to a proper understanding of these spectra. Additionally, the use of polyad matrices to allow for intensity sharing is integral to the correct treatment of anharmonic intensities in PAHs. Combined with the previous publication[16] of the absorption spectra of phenylacetylene and d_1-phenylacetylene in the CH (CD) stretch fundamental region, the full absorption spectrum up to 3400 and 3100 cm^{-1}, respectively, excluding the 2300–2500 cm^{-1} region that is outside of the laser frequency capabilities of FELIX, is now complete and included in Fig. S3.

Overall, very good agreement is present between experiment and theory for both phenylacetylene and d_1-phenylacetylene, with an average difference in frequency of 1.2% and 1.0%, respectively, for the directly assigned features. The low-frequency rocking and bending motions at ~500 cm^{-1} and below have some of the largest differences in frequency, with an average difference of 2.5% and

2.7%, respectively. These modes are notoriously difficult to characterize with computational methods, and all of them deviate in a similar manner. Even so, an assignment is still easy to make for all features due to the sparsity of features in this region. As described in Sec. III A, ν_{21} and $2\nu_{21}$ in phenylacetylene show the largest deviation in frequency between theory and experiment (3.8% and 6.1%), with the inaccuracy compounded for the overtone transition. This same deviation is not observed in d_1-phenylacetylene. The average difference on the order of 1% for these molecules is larger than that found for unsubstituted[18] and methyl-substituted[19] PAHs. This is not so surprising given the strong coupling present in phenylacetylene[16] and the known difficulty in computing the vibrational spectra of acetylene molecules.[42]

Large isotopic frequency shifts are reported here for various modes that involve the acetylene hydrogen. Many of these modes either lose or gain intensity based on deuteration, causing major changes to the resultant absorption spectrum, particularly in the 500–900 cm^{-1} (20–11.1 μm) range. Further experiments on isotopically labeled PAHs are needed, and such absorption experiments are currently underway in our laboratory. Even with the insights provided herein, there remain quite a number of unanswered questions regarding how deuteration impacts the emission of PAHs, especially with regard to the strong infrared bands observed in the 1–20 μm range.[1,2,48] Very little PAH, and their deuterated isotopologues in particular, emission data exist in the literature. A recent emission experiment on phenylacetylene and d_1-phenylacetylene carried out by Lacinbala *et al.*[49] and a follow-up computational study by our group[16] look into the role that anharmonicity plays in the emission of substituted aromatic molecules. Outside of this recent example, there exists a dearth of experimental emission data for this wavelength region, requiring further experimental and computational investigation to understand how anharmonicity and the isotopic frequency and intensity shifts impact the emission spectrum of standard and functionalized PAHs, molecules that are strongly tied to infrared observations pertinent to astronomical observation during the age of JWST and its possible successors.

SUPPLEMENTARY MATERIAL

See the supplementary material for the expanded view of the overlapping features at 475.7 and 480.6 cm^{-1} in the experimental spectrum of d_1-phenylacetylene, the 2- vs 3-quanta spectrum of d_1-phenylacetylene, the complete mid- to far-IR absorption spectrum of phenylacetylene and d_1-phenylacetylene excluding the 2300–2500 cm^{-1} region, and the complete tabulation of the computational frequencies for both molecules.

ACKNOWLEDGMENTS

V.J.E. acknowledges an appointment to the NASA Postdoctoral Program at NASA Ames Research Center, administered by the Oak Ridge Associated Universities through a contract with NASA. C.B. is grateful for an appointment at the NASA Ames Research Center through the San José State University Research Foundation (Grant No. 80NSSC22M0107). V.J.E., C.B., and R.C.F. acknowledge support from the Internal Scientist Funding Model (ISFM) Laboratory Astrophysics Directed Work Package at NASA Ames. Computer time from the Pleiades cluster of the NASA Advanced Supercomputer (NAS) is gratefully acknowledged. R.C.F. acknowledges support from NASA under Grant No. NNH22ZHA004C and the Mississippi Center for Supercomputing Research, supported in part by NSF under Grant No. OIA-1757220. Studies of interstellar PAHs at Leiden Observatory are supported through a NWO Spinoza grant. The HFML-FELIX Laboratory is supported by the project CALIPSOplus under Grant Agreement No. 730872 from the EU Framework Program for Research and Innovation Horizon 2020. We gratefully acknowledge the Nederlandse Organisatie voor Wetenschappelijk Onderzoek (NWO) and acknowledge the FELIX staff.

AUTHOR DECLARATIONS

Conflict of Interest

The authors have no conflicts to disclose.

Author Contributions

Vincent J. Esposito: Conceptualization (equal); Data curation (equal); Formal analysis (equal); Funding acquisition (equal); Investigation (equal); Methodology (equal); Project administration (equal); Resources (equal); Software (equal); Validation (equal); Visualization (equal); Writing – original draft (equal); Writing – review & editing (equal). **Piero Ferrari**: Data curation (equal); Formal analysis (equal); Investigation (equal); Methodology (equal); Validation (equal); Visualization (equal); Writing – original draft (equal); Writing – review & editing (equal). **Wybren Jan Buma**: Data curation (equal); Formal analysis (equal); Funding acquisition (equal); Supervision (equal); Writing – review & editing (equal). **Ryan C. Fortenberry**: Funding acquisition (equal); Supervision (equal); Writing – review & editing (equal). **Christiaan Boersma**: Funding acquisition (equal); Resources (equal); Supervision (equal); Writing – review & editing (equal). **Alessandra Candian**: Methodology (equal); Supervision (equal); Writing – review & editing (equal). **Alexander G. G. M. Tielens**: Conceptualization (equal); Supervision (equal); Writing – review & editing (equal).

DATA AVAILABILITY

The data that support the findings of this study are available in the supplementary material and from the corresponding author upon reasonable request.

REFERENCES

[1] A. G. G. M. Tielens, "Interstellar polycyclic aromatic hydrocarbon molecules," Annu. Rev. Astron. Astrophys. **46**, 289–337 (2008).
[2] C. Boersma, L. J. Allamandola, V. J. Esposito, A. Maragkoudakis, J. D. Bregman, P. Temi, T. J. Lee, R. C. Fortenberry, and E. Peeters, "JWST: Deuterated PAHs, PAH nitriles, and PAH overtone and combination bands. I. Program description and first look," Astrophys. J. **959**(2), 74 (2023).
[3] M. L. Laury, M. J. Carlson, and A. K. Wilson, "Vibrational frequency scale factors for density functional theory and the polarization consistent basis sets," J. Comput. Chem. **33**(30), 2380–2387 (2012).

[4]S. R. Langhoff, "Theoretical infrared spectra for polycyclic aromatic hydrocarbon neutrals, cations, and anions," J. Phys. Chem. **100**(8), 2819–2841 (1996).
[5]C. W. Bauschlicher and S. R. Langhoff, "The calculation of accurate harmonic frequencies of large molecules: The polycyclic aromatic hydrocarbons, a case study," Spectrochim. Acta, Part A **53**(8), 1225–1240 (1997).
[6]C. W. Bauschlicher, C. Boersma, A. Ricca, A. L. Mattioda, J. Cami, E. Peeters, F. Sánchez de Armas, G. Puerta Saborido, D. M. Hudgins, and L. J. Allamandola, "The NASA AMES polycyclic aromatic hydrocarbon infrared spectroscopic database: The computed spectra," Astrophys. J., Suppl. Ser. **189**(2), 341 (2010).
[7]C. W. Bauschlicher, A. Ricca, C. Boersma, and L. J. Allamandola, "The NASA Ames PAH IR spectroscopic database: Computational version 3.00 with updated content and the introduction of multiple scaling factors," Astrophys. J., Suppl. Ser. **234**(2), 32 (2018).
[8]O. Pirali, M. Vervloet, G. Mulas, G. Malloci, and C. Joblin, "High-resolution infrared absorption spectroscopy of thermally excited naphthalene. Measurements and calculations of anharmonic parameters and vibrational interactions," Phys. Chem. Chem. Phys. **11**(18), 3443–3454 (2009).
[9]F. M. Behlen, D. B. McDonald, V. Sethuraman, and S. A. Rice, "Fluorescence spectroscopy of cold and warm naphthalene molecules: Some new vibrational assignments," J. Chem. Phys. **75**(12), 5685–5693 (1981).
[10]E. Cané, P. Palmier, R. Tarroni, A. Trombetti, and N. C. Handy, "The high-resolution infrared spectra of naphthalene-h8 and naphthalene-d8: Comparison of scaled SCF and density functional force fields," Gazz. Chim. Ital. **126**(5), 289–296 (1996).
[11]J. M. Bakker, B. Redlich, A. F. G. Van Der Meer, and J. Oomens, "Infrared spectroscopy of gas-phase polycyclic aromatic hydrocarbon cations in the 10–50 μm spectral range," Astrophys. J. **741**(2), 74 (2011).
[12]J. Roithová, J. Jašík, J. J. D. P. Mellado, and D. Gerlich, "Electronic spectra of ions of astrochemical interest: From fast overview spectra to high resolution," Faraday Discuss. **217**, 98–113 (2019).
[13]S. D. Wiersma, A. Candian, J. M. Bakker, and A. Petrignani, "Gas-phase spectroscopy of photostable PAH ions from the mid- to far-infrared," Mon. Not. R. Astron. Soc. **516**(4), 5216–5226 (2022).
[14]A. K. Lemmens, P. Ferrari, D. Loru, G. Batra, A. L. Steber, B. Redlich, M. Schnell, and B. Martinez-Haya, "Wetting of a hydrophobic surface: Far-IR action spectroscopy and dynamics of microhydrated naphthalene," J. Phys. Chem. Lett. **14**, 10794 (2023).
[15]V. J. Esposito, L. J. Allamandola, C. Boersma, J. D. Bregman, R. C. Fortenberry, A. Maragkoudakis, and P. Temi, "Anharmonic IR absorption spectra of the prototypical interstellar PAHs phenanthrene, pyrene, and pentacene in their neutral and cation states," Mol. Phys. e2252936 (2023).
[16]V. J. Esposito, P. Ferrari, W. J. Buma, C. Boersma, C. J. Mackie, A. Candian, R. C. Fortenberry, and A. G. G. M. Tielens, "Anharmonicity and deuteration in the IR absorption and emission spectrum of phenylacetylene," Mol. Phys. e2261570 (2023).
[17]C. J. Mackie, A. Candian, X. Huang, E. Maltseva, A. Petrignani, J. Oomens, W. J. Buma, T. J. Lee, and A. G. G. M. Tielens, "The anharmonic quartic force field infrared spectra of three polycyclic aromatic hydrocarbons: Naphthalene, anthracene, and tetracene," J. Chem. Phys. **143**(22), 224314 (2015).
[18]C. J. Mackie, A. Candian, X. Huang, E. Maltseva, A. Petrignani, J. Oomens, A. L. Mattioda, W. J. Buma, T. J. Lee, and A. G. G. M. Tielens, "The anharmonic quartic force field infrared spectra of five non-linear polycyclic aromatic hydrocarbons: Benz[a]anthracene, chrysene, phenanthrene, pyrene, and triphenylene," J. Chem. Phys. **145**(8), 084313 (2016).
[19]C. J. Mackie, A. Candian, X. Huang, E. Maltseva, A. Petrignani, J. Oomens, W. Jan Buma, T. J. Lee, and A. G. G. M. Tielens, "The anharmonic quartic force field infrared spectra of hydrogenated and methylated PAHs," Phys. Chem. Chem. Phys. **20**(2), 1189–1197 (2018).
[20]C. J. Mackie, T. Chen, A. Candian, T. J. Lee, and A. G. G. M. Tielens, "Fully anharmonic infrared cascade spectra of polycyclic aromatic hydrocarbons," J. Chem. Phys. **149**(13), 134302 (2018).
[21]C. J. Mackie, A. Candian, T. J. Lee, and A. G. G. M. Tielens, "Anharmonicity and the IR emission spectrum of neutral interstellar PAH molecules," J. Phys. Chem. A **126**(20), 3198–3209 (2022).
[22]S. Banhatti, D. B. Rap, A. Simon, H. Leboucher, G. Wenzel, C. Joblin, B. Redlich, S. Schlemmer, and S. Brünken, "Formation of the acenaphthylene cation as a common C_2H_2-loss fragment in dissociative ionization of the PAH isomers anthracene and phenanthrene," Phys. Chem. Chem. Phys. **24**(44), 27343–27354 (2022).
[23]G. Mulas, C. Falvo, P. Cassam-Chenaï, and C. Joblin, "Anharmonic vibrational spectroscopy of polycyclic aromatic hydrocarbons (PAHs)," J. Chem. Phys. **149**(14), 144102 (2018).
[24]R. Chown, A. Sidhu, E. Peeters, A. G. G. M. Tielens, C. Jan, O. Berne, E. Habart, F. Alarcon, A. Canin, I. Schroetter *et al.*, "PDRs4AII IV. An embarrassment of riches: Aromatic infrared bands in the Orion bar," arXiv:2308.16733 (2023).
[25]E. Maltseva, A. Petrignani, A. Candian, C. J. Mackie, X. Huang, T. J. Lee, G. Alexander, G. M. Tielens, J. Oomens, and W. Jan Buma, "High-resolution IR absorption spectroscopy of polycyclic aromatic hydrocarbons: The realm of anharmonicity," Astrophys. J. **814**(1), 23 (2015).
[26]E. Maltseva, A. Petrignani, A. Candian, C. J. Mackie, X. Huang, T. J. Lee, G. Alexander, G. M. Tielens, J. Oomens, and W. Jan Buma, "High-resolution IR absorption spectroscopy of polycyclic aromatic hydrocarbons in the 3 μm region: Role of periphery," Astrophys. J. **831**(1), 58 (2016).
[27]E. Maltseva, C. J. Mackie, A. Candian, A. Petrignani, X. Huang, T. J. Lee, G. Alexander, G. M. Tielens, J. Oomens, and W. Jan Buma, "High-resolution IR absorption spectroscopy of polycyclic aromatic hydrocarbons in the 3 μm region: Role of hydrogenation and alkylation," Astron. Astrophys. **610**, A65 (2018).
[28]A. K. Lemmens, D. B. Rap, J. M. M. Thunnissen, C. J. Mackie, A. Candian, A. G. G. M. Tielens, A. M. Rijs, and W. J. Buma, "Anharmonicity in the mid-infrared spectra of polycyclic aromatic hydrocarbons: Molecular beam spectroscopy and calculations," Astron. Astrophys. **628**, A130 (2019).
[29]A. K. Lemmens, A. M. Rijs, and W. J. Buma, "Infrared spectroscopy of jet-cooled 'GrandPAHs' in the 3–100 μm region," Astrophys. J. **923**(2), 238 (2021).
[30]D. Loru, C. Cabezas, J. Cernicharo, M. Schnell, and A. L. Steber, "Detection of ethynylbenzene in TMC-1 and the interstellar search for 1,2-diethynylbenzene," Astron. Astrophys. **677**, A166 (2023).
[31]V. Yatsyna, D. J. Bakker, P. Salén, R. Feifel, A. M. Rijs, and V. Zhaunerchyk, "Infrared action spectroscopy of low-temperature neutral gas-phase molecules of arbitrary structure," Phys. Rev. Lett. **117**(11), 118101 (2016).
[32]S. Jaeqx, J. Oomens, A. Cimas, M.-P. Gaigeot, and A. M. Rijs, "Gas-phase peptide structures unraveled by far-IR spectroscopy: Combining IR-UV ion-dip experiments with Born–Oppenheimer molecular dynamics simulations," Angew. Chem., Int. Ed. **53**(14), 3663–3666 (2014).
[33]S. Bakels, M.-P. Gaigeot, and A. M. Rijs, "Gas-phase infrared spectroscopy of neutral peptides: Insights from the far-IR and THz domain," Chem. Rev. **120**(7), 3233–3260 (2020).
[34]A. D. Becke, "Density-functional thermochemistry. III. The role of exact exchange," J. Chem. Phys. **98**(7), 5648–5652 (1993).
[35]V. Barone, P. Cimino, and E. Stendardo, "Development and validation of the B3LYP/N07D computational model for structural parameter and magnetic tensors of large free radicals," J. Chem. Theory Comput. **4**(5), 751–764 (2008).
[36]M. J. Frisch, G. W. Trucks, H. B. Schlegel, G. E. Scuseria, M. A. Robb, J. R. Cheeseman, G. Scalmani, V. Barone, G. A. Petersson, H. Nakatsuji *et al.*, Gaussian 16, 2016.
[37]V. Barone, M. Biczysko, and J. Bloino, "Fully anharmonic IR and Raman spectra of medium-size molecular systems: Accuracy and interpretation," Phys. Chem. Chem. Phys. **16**(5), 1759–1787 (2014).
[38]V. Barone, "Anharmonic vibrational properties by a fully automated second-order perturbative approach," J. Chem. Phys. **122**(1), 014108 (2005).
[39]R. C. Fortenberry and T. J. Lee, "Chapter six—Computational vibrational spectroscopy for the detection of molecules in space," Annu. Rep. Comput. Chem. **15**, 173–202 (2019).
[40]P. R. Franke, J. F. Stanton, and G. E. Douberly, "How to VPT2: Accurate and intuitive simulations of CH stretching infrared spectra using VPT2+K with large

effective Hamiltonian resonance treatments," J. Phys. Chem. A **125**(6), 1301–1324 (2021).
[41]J. K. G. Watson, *On Vibrational Spectra and Structure* (Elsevier, Amsterdam, 1977).
[42]R. C. Fortenberry and T. J. Lee, "Vibrational and rovibrational spectroscopy applied to astrochemistry," in *Vibrational Dynamics of Molecules* (World Scientific, 2022), pp. 235–295.
[43]J. F. Gaw, A. Willets, W. H. Green, and N. C. Handy, "SPECTRO—A program for the derivation of spectrscopic constants from provided quartic force fields and cubic dipole fields," in *Advances in Molecular Vibrations and Collision Dynamics*, edited by J. M. Bowman and M. A. Ratner (JAI Press, Inc., Greenwich, CT, 1991), pp. 170–185.
[44]J. M. L. Martin and P. R. Taylor, "Accurate ab initio quartic force field for *trans*-HNNH and treatment of resonance polyads," Spectrochim. Acta, Part A **53**(8), 1039–1050 (1997).
[45]J. M. L. Martin, T. J. Lee, P. R. Taylor, and J. P. François, "The anharmonic force field of ethylene, C_2H_4, by means of accurate ab initio calculations," J. Chem. Phys. **103**(7), 2589–2602 (1995).
[46]T. J. Lee and R. C. Fortenberry, "The unsolved issue with out-of-plane bending frequencies for C=C multiply bonded systems," Spectrochim. Acta, Part A **248**, 119148 (2021).
[47]R. C. Fortenberry, T. J. Lee, and H. S. P. Müller, "Excited vibrational level rotational constants for SiC_2: A sensitive molecular diagnostic for astrophysical conditions," Mol. Astrophys. **1**, 13–19 (2015).
[48]E. Peeters, S. Hony, C. Van Kerckhoven, A. G. G. M. Tielens, L. J. Allamandola, D. M. Hudgins, and C. W. Bauschlicher, "The rich 6 to 9 μm spectrum of interstellar PAHs," Astron. Astrophys. **390**(3), 1089–1113 (2002).
[49]O. Lacinbala, G. Féraud, J. Vincent, and T. Pino, "Aromatic and acetylenic C–H or C–D stretching bands anharmonicity detection of phenylacetylene by UV laser-induced vibrational emission," J. Phys. Chem. A **126**(30), 4891–4901 (2022).